The Influence of a Polymeric Nucleating Additive on the Crystallisation in Glass Fibre Reinforced Polyamide 6 Composites

U. Göschel, W. Lutz, N.C. Davidson

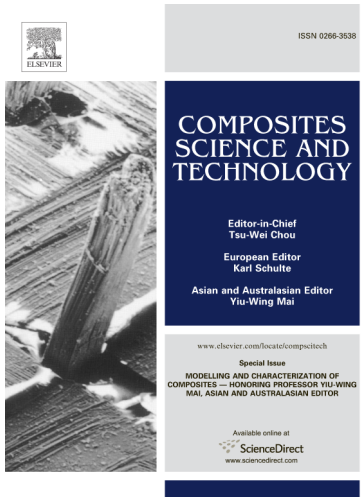

The Influence of a Polymeric Nucleating Additive on the Crystallisation in Glass Fibre Reinforced Polyamide 6 Composites

U. Göschel, W. Lutz, N.C. Davidson

PII: S0266-3538(06)00463-5
DOI: 10.1016/j.compscitech.2006.12.005
Reference: CSTE 3549

To appear in: *Composites Science and Technology*

Received Date: 14 December 2005
Revised Date: 4 December 2006
Accepted Date: 6 December 2006

Please cite this article as: U. Göschel, W. Lutz, N.C. Davidson, The Influence of a Polymeric Nucleating Additive on the Crystallisation in Glass Fibre Reinforced Polyamide 6 Composites, *Composites Science and Technology* (2006), doi: 10.1016/j.compscitech.2006.12.005

The Influence of a Polymeric Nucleating Additive on the Crystallisation in Glass Fibre Reinforced Polyamide 6 Composites

U. Göschel[1)], W. Lutz[2)], and N.C. Davidson[3)]

[1)] University of Stuttgart, Institute for Polymer Technology (IKT), Pfaffenwaldring 32, 70569 Stuttgart, Germany, email ulrich.goeschel@ikp.uni-stuttgart.de, phone +49 711 685-62024, fax +49 711 685-62066

[2)] present address: University of Stuttgart, Institute for Materials Testing, Materials Science and Strength of Materials (IMWF), Pfaffenwaldring 32, 70569 Stuttgart, Germany

[3)] present address: Malvern Instruments Limited, Enigma Business Park, Grovewood Rd., Malvern, WR14 1XZ, Great Britain

Abstract

Short glass fibre reinforced polyamide 6 composites compounded with a polymeric nucleating additive based on polyamide 2.2 of different content (0, 0.1 and 0.2 wt-%) and processed by injection moulding have been studied to characterise the additive effect on the crystallisation kinetics and morphology. Differential scanning calorimetrical and optical hot stage experiments have shown a significant increase in the overall crystallisation rate as well as the spherulitic growth nucleating additive. Additionally, the presence of glass fibres is proven to enhance crystallisation. Atomic force microscopy confirms the

existence of a transcrystalline layer in the vicinity of the glass fibres. The nucleating additives have significantly decreased the spherulitic size from about 15 to 20 µm towards less than 5 µm, which leads to an improved fibre-to-matrix contact. Those morphological changes are seen as the reason for a strong increase in the Martens heat deflection temperature from 145 to 164 °C characterising an improved thermal stability.

KEY WORDS: A Polymer-matrix composites (PMCs), B Interface, B Microstructure, B Nucleation, E Injection moulding

1 Introduction

The crystallisation behaviour of glass fibre reinforced thermoplastic composites is affected by the materials chosen (polymeric matrix, glass fibre, sizing), the use of nucleating additives as well as the thermal and mechanical conditions during processing and the practical use. During solidification from the melt, the existence of both a gradient in orientation (matrix and fibre) and temperature (core and surface) has a large impact on the structural formation (rate and morphology) and resulting product properties. The complex nature of those parameters can be demonstrated by the presence of differential shrinkage and residual stresses leading to the effect of warpage, which is characteristic for fibre reinforced thermoplastic composites. The structural development during solidification is known to be described as primary crystallisation consisting of nucleation and crystal growth leading to a defined degree of crystallinity depending on the crystallisation conditions applied. Moreover, the long-term process of completion of crystallisation is widely considered as secondary crystallisation to reach the final morphology and resulting properties.

With respect to Alfonso and Ziabicki [1], the primary crystallisation includes the growth of predetermined nuclei as well as sporadic thermal nucleation (N_{th}) followed by growth. The predetermined nuclei (N_0) defined as already be present at the start of the crystallisation consist of heterogeneous (N_{het}) and athermal homogeneous nuclei (N_{ath}). Consequently, the total number of growing nuclei (N_{tot}) at any time (t) can be expressed [1] by

$$N_{tot}(t) = N_{het} + N_{ath} + \int_0^t N_{th}\, dt \qquad (1)$$

The heterogeneous nuclei are mainly related to the use of nucleating additives.

Catalysts, pigments or impurities are also considered as heterogeneous nuclei, which may enhance crystallisation too. The athermal nuclei strongly depend on the thermal and deformation history of the melt related to the formation of crystal fragments and chain clusters [1]. Those memory effects can be eliminated by appropriate annealing conditions in the melt. However, the required high temperature and annealing time have to be carefully determined. In the case of PA 6, the effects from degradation starting already at low melt temperatures exceeding 260 °C as well as hydrogen bonding are to be considered.

The use of nucleating additives is essential in industrial processing to control the structure formation and to shorten the cycle time. According to Titzschkau and Beck [2], inorganic compounds (minerals such as talc or kaolin) and organic compounds (e.g. salts of mono- or polycarbonic acids such as Ca-stearate, Ca-montanate, Li-montanate, Na-benzoate, di-benzylidene sorbitols or salts of phosphorous esters) are used as nucleating additives for PA 6. Furthermore, oligomers of the caprolactam and polymers such as PA 2.2 [2, 3] or PA 4.6 [2, 4] are known to enhance nucleation.

Due to low costs and acceptable nucleation efficiency of talc and kaolin [5] those materials have been played a major role in industrial processing of PA 6 over years. However, the required homogeneous dispersion of small particle sizes to achieve the anticipated fine crystalline structure remains complex. In the case of organic nucleating compounds well-distributed and small crystalline entities will be achieved during cooling of a completely molten PA 6 [2]. Recently, the nucleating efficiency of the polymeric additive Brueggolen® P22, based on polyamide 2.2, as compounded during injection moulding of the PA 6

homopolymer Ultramid B3 has been proven in preliminary investigations [6] and by WAXD synchrotron studies at the ANKA Synchrotron Radiation Facility in Karlsruhe [7].

In the present study, the main focus will be given to the effect of nucleating additive Brueggolen® P22 content on the primary crystallisation of glass fibre reinforced polyamide (PA 6-GF30) of a given fibre geometry and sizing, processed by injection moulding at optimised conditions for melt temperature, holding pressure and mould temperature.

2 Experimental

2.1 Material

A commercial 30 wt-% short glass fibre reinforced polyamide (PA 6-GF30) grade Bergamid B70G30 with a fibre diameter of 10 to 13 µm and a fibre length of 3.2 to 4.5 mm in the granule was used. Prior to processing, 0.2 wt-% Ca stearate and the polymeric nucleating additive Brueggolen® P22 (denoted as P22 in the following) at different content of 0, 0.1 and 0.2 wt-% was added to the PA 6 in a powdered form during compounding. The PA 2.2, which is the chemical basis for the P22, is the condensation product of oxalic acid derivatives with ethylene diamine (Figure 1). The polymerisation degree of the used nucleating additive is as low as about 10 [2]. Due to only two CH_2-sequences in the monomeric unit of PA 2.2 compared to five in PA 6 an extraordinary large number of hydrogen bonds between the NH and the CO groups can be established, which leads to a high thermal stability of PA 2.2 with no melting up to its decomposition temperature of about 400 °C.

Tensile bars (150 x 10 x 4 mm^3) with respect to DIN EN ISO 527 as well as rectangular plates (61 x 61 x 2 mm^3) according to DIN EN ISO 294-4 were processed using an injection moulding machine DEMAG ergotec 60/370-120. The processing conditions based on a parameter study by Fracassi [8] are given in Table 1.

2.2 Methods

2.2.1 Fibre Orientation

The measurements were performed on tensile bars and rectangular plates as well. From the tensile bars an area perpendicular to the processing direction was used (Figure 2). The measurement was performed on about 16,000 fibres and exhibits a statistical reliability. The fibre orientation was measured from polished sample sections applying an image analysis system designed in house. The normalised first moments for a two dimensional image are used to find the centre of the object while information on size, orientation and ellipticity of the object were derived from the second moments, equ. (2), see Davidson [9]. By using a calibrated xy translation stage and overlapping image frames according to Davidson et al. [10], the fibre orientation with respect to position in the sample could be accurately determined.

$$\tan 2\phi = \frac{2M_{xy}}{(M_{xx} - M_{yy})}$$

$$a^2 = 2(M_{xx} + M_{yy}) + 2\sqrt{\left[(M_{xx} - M_{yy})^2 + 4M_{xy}^2\right]}$$

$$b^2 = 2(M_{xx} + M_{yy}) - 2\sqrt{\left[(M_{xx} - M_{yy})^2 + 4M_{xy}^2\right]}$$

(2)

Where:

ϕ = in plane angle

a = semi-major axis length

b = semi-minor axis length

θ = out of plane angle

$$\theta = \cos^{-1}\left(\frac{b}{a}\right)$$

2.2.2 Thermal Analysis

Differential scanning calorimetry (DSC) was performed by a Mettler DSC 821 operating with the software STAR V6.10. The sample mass was about 7 mg. Subsequent to a heating run from -50 to 260 °C at 10 K/min and an annealing at 260 °C for two minutes a cooling run to room temperature at 10 K/min followed by a second heating run to 260 °C at 10 K/min was performed. Nitrogen atmosphere at a flow rate of 80 ml/min was chosen to avoid degradation.

2.2.3 Isothermal Crystallisation Studies

Crystallisation kinetics was investigated under isothermal conditions using differential scanning calorimetry (DSC) and hot stage polarised light microscopy (HSM) characterising the crystallisation rate from the exothermal peak and spherulitic growth, respectively. In both cases a temperature profile according to Figure 3 was applied, see Moritz [11]. Starting from 23 °C the temperature was raised to the melting stage (T_m) at 265 °C using a rate of 50 K/min. The melt was annealed for three minutes in order to eliminate aggregation and crystal clusters originated from thermal and mechanical loading history, which may substantially affect crystallisation. Thereafter, rapid cooling at 80 K/min to the given temperature for isothermal crystallisation (T_c) ranging from 201 to 211 °C was used.

Differential Scanning Calorimetry (DSC)

For the DSC experiments (Mettler DSC 821) a sample mass of about 5 mg was chosen. The time-dependent development of the degree of crystallinity $\chi(t)$ was determined from the heat flow dQ/dt of the exothermal crystallisation peak by means of equ. (3) assuming that the primary crystallisation is completed in the time range from t_0 to t leading to $\chi(t)$ ranging from 0 to 100 %. According to equ. (3), $\chi(t)$ can also be expressed by the increase of the crystallisation enthalpy (ΔH_c) with time (t) divided by the corresponding crystallisation enthalpy of ideal crystals (ΔH_c^0), see Azzuri [12].

$$\chi(t) = \frac{\int_{t_0}^{t} \frac{dQ}{dt} dt}{\int_{t_0}^{\infty} \frac{dQ}{dt} dt} = \frac{\Delta H_c(t)}{\Delta H_c^0} \qquad (3)$$

In order to describe quantitatively the crystallisation process under isothermal conditions, where both nucleation and crystal growth are assumed to be time-independent, the Avrami equation can be used, which reads for heterogeneous nucleation as

$$\chi(t) = 1 - \exp(-k \cdot t^n) \qquad (4)$$

Here, the Avrami parameter $k = f(T_C)$ relates to the overall crystallisation rate and (n) to the nucleation mechanism, which includes information on the growth dimensionality and the type of nucleation. A linearisation of equ. (4) leads to equ. (5), which enables a simple determination of (k) and (n) from the intersection with the ordinate and the slope in the lower log t range, respectively, see e.g. Chrisholm and Zimmer [13] and Hiemenz [14].

$$\log[-\ln(1-\chi)] = \log k + n \log t \qquad (5)$$

The Avrami equation is the most applied tool to describe the phenomenology of the crystal development. However, any insight into the molecular processes related to nucleation and crystal growth cannot be given [12]. For simplicity, the Avrami equation supposes a radial growth of crystals at constant rate without any interaction with neighbouring crystals. Moreover, it requires a complete phase transformation without a change in volume, a uniform nucleation, a constant density and shape of the growing nuclei. At least, it excludes the secondary crystallisation, see Verhoven [15].

The crystallisation rate can be described by the half width $t_{1/2}$, which is defined as the time to reach $\chi(t) = 0.5$ of the overall crystallisation, equ. (6):

$$t_{1/2} = \left[\frac{\ln 2}{k}\right]^{\frac{1}{n}} \tag{6}$$

The Avrami parameters k and n in equ. (6) correspond to those in equ. (5). The value $\chi(t) = 0.5$ can be obtained from the experimental s-shaped curve degree of crystallinity (χ) depending on the crystallisation time (t).

Furthermore, the time-to-peak (t_p), where the overall crystallisation rate reaches a maximum can be determined from the minimum of the exothermal crystallisation peak of the isothermal DSC traces. With respect to Alfonso and Ziabicki [1], the time-to-peak is related to the number of predetermined nuclei (N_0), equ. (7).

$$t_p = \text{const.}\ N_0^{-1/3} \tag{7}$$

At the start of crystallisation, the predetermined number of nuclei includes the heterogeneous nuclei (N_{het}) as well as the athermal nuclei (N_{ath}), compare with equ. (1).

Hot Stage Polarised Light Microscopy (HSM)

A Leitz DM LB microscope from Leica was used together with a Linkam TMS94 heating cell. The sample with a thickness of 40 to 50 µm was placed between a polariser-analyser set-up in transmission mode [11]. To avoid thermal decomposition a flow of nitrogen gas was applied. For statistical reasons each measurement was repeated three times at the same conditions. During isothermal crystallisation at the given crystallisation temperatures (T_c) in the chosen range from 201 to 211 °C, the transmitted light intensity I (t) increases with the spherulitic growth. In the molten stage at I (t = 0) the transmitted intensity is zero and reaches a plateau at t = ∞, where the primary crystallisation is completed. From the intensity values the relative degree of crystallinity χ_{rel} (t) can be calculated according to equ. (8).

$$\chi_{rel}(t) = \frac{I(t) - I(t=0)}{I(t=\infty) - I(t=0)} \qquad (8)$$

Consequently, the experimental curve I = f (t) provides the half-width ($t_{1/2}$), which corresponds to χ_{rel} = 50 %, compare equ. (6).

2.2.4 Light Microscopy (LM)

Polarised light microscopy studies in transmission mode were performed on thin microtom slices with a thickness of about 100 µm by a Leitz DM RXP microscope from Leica. The cuts were performed with a microtom Polycut E from Reichert Jung at room temperature.

2.2.5 Scanning Electron Microscopy (SEM)

For investigation of the morphology with SEM, tensile bars were prepared via cryo fracture. The samples were cracked under nitrogen atmosphere, both parallel as well as normal to the processing direction (Figure 2) and then gold sputtered. Further samples resulted from a tensile experiment at room temperature according to DIN EN ISO 527. The cross-section of the samples was investigated by means of a Jeol JSM 6300 F microscope operating at an acceleration voltage of 10 kV and an angle of 30°.

2.2.6 Atomic Force Microscopy (AFM)

Pulsed Force Mode (PFM)

The PFM is an external module for AFM from WITec GmbH, Germany. Using this method it is possible to map images of topography, adhesion and stiffness simultaneously as discussed by Krotil et al. [16]. The PFM applies a sinusoidal modulation on the vertical piezo of the AFM. At each data point a complete force-to-distance cycle was performed providing the stiffness from the slope of the curve. The lowest force of the curve characterises the maximum adhesive force (or pull-off force). The PFM is an intermittent contact mode and has the main advantages of low contact time, low lateral shear forces acting between probe and sample and the possibility to control the forces applied on the sample which enables the imaging of soft samples such as polymers [17].

Measuring Conditions and Sample Preparation

The atomic force microscopic data were obtained on an Explorer from TopoMetrix. The experiments were performed using the pulsed force mode in ambient air at 500 kHz. A rectangular silicon cantilever (2.82 x 25 x 225 μm^3)

with a free resonance frequency of 73 kHz and a stiffness of 2.1 N/m from Nanosensors was used. The radius of curvature of the tip was approximately 10 nm. Samples of each material for AFM were cut perpendicular and parallel to the processing direction according to Figure 3. Thereafter, the samples were embedded in epoxy resin and subsequently polished by abrasive paper ranging from FEPA norm 320 to 4000 (grain size 46 to 5 µm) followed by a diamond polishing paste with a grain size of 1 µm and ultrasonic bath cleaning.

2.2.7 Martens Heat Deflection Temperature (HDT)

The Martens heat deflection temperature (HDT) was determined on sections of tensile bars according to DIN 53462 applying a bending stress during heating at a slow rate of 50 K/hour starting from room temperature. The HDT corresponds to the temperature at a given tensile bar deflection of about 0.2 % according to DIN 53462.

3. Results

3.1 Fibre Orientation

The measurements were carried out on tensile bars as well as rectangular plates.

Tensile Bar

The PA 6-GF30 samples of different additive content (0, 0.1 and 0.2 wt-%) have shown a preferential alignment of the fibres parallel to the processing direction, expressed by a_{11} (Table 2). The parameter a_{11} ranges between 0.677 and 0.700 and reveals a small increase with increasing nucleating additive content. The fibre orientation in the plane 1-2, perpendicular to the processing direction is

much lower. The corresponding parameter varies between 0.188 and 0.201. With respect to the limited thickness of 4 mm, the fibre orientation along the thickness (a_{33}) is very small and ranges between 0.111 and 0.123. It can be concluded, that the effect of the nucleating additive content (0, 0.1 and 0.2 wt - %) on the fibre orientation applying identical processing conditions can almost be neglected.

Rectangular Plate

By the example of the 0.1 wt-% nucleated PA 6-GF30, the a_{22} component of the second order orientation tensor is represented in the plane 2-3, which corresponds the plate area of 61 x 2 mm^2. (Figure 5). The higher the value of a_{22}, the more the fibres are oriented perpendicular to the processing direction. Consequently, in the core region the fibres have a preferential orientation perpendicular to the processing direction (along the 2-axis) with a_{22} close to 1. Approaching the surface region, the a_{22} value decreases down to about 0.2, which goes along with a preferential fibre orientation parallel to the processing direction. The a_{33} component has been found to be negligible. Thus the a_{11} component is approximately the negative of the above plot. All three samples (0, 0.1 and 0.2 wt-% nucleated) have shown almost the same fibre orientation distribution with a classic 'core' region of comparable size. Consequently, any differences in the thermo-mechanical behaviour will not be related to the fibre orientation.

3.2 Thermal Analysis

The melting peak temperature as determined from the first temperature run of DSC measurements is about 222 °C and does not change with the P22 additive

content (Table 3). The corresponding melting enthalpy and thus the degree of crystallinity calculated from the measured melting enthalpy divided by the melting enthalpy of ideal crystals $\Delta H_{crystal}$ = 188.4 J/g according to Wunderlich [19] seems to be somewhat higher for nucleated compared to the non-nucleated samples. The degree of crystallinity of 32 % and 32.5 % for a P22 content of 0 and 0.1 as well as 0.2 wt-%, respectively (Table 3) is in the normal range of PA 6 GF30 materials. The additive effect is seen more pronounced in the onset of crystallisation leading to 192.4, 194.1 and 194.6 °C for a P22 content of 0, 0.1 and 0.2 wt-%, respectively (Table 3) by applying an identical cooling rate of 10 K/min. Those findings are in good agreement with isothermal DSC results in chapter 3.3.1.

3.3 Isothermal Crystallisation

Two different methods namely the differential scanning calorimetry (DSC) and the hot stage polarised light microscopy (HSM) were applied. Despite of large differences in the underlaying phenomena that are the heat flow (DSC) and spherulitic growth (HSM), both methods are complementary in describing the phenomenon of the primary crystallisation.

3.3.1 Differential Scanning Calorimetry (DSC)

The time-to-peak (t_p) as determined from the exothermal crystallisation peak during isothermal crystallisation according to equ. (7) is related to the number of predetermined nuclei (N_0). At the crystallisation temperature of 205 °C, the value t_p decreases from 8.2 min (0 wt-%) over 6.1 min (0.1 wt-%) to 5.9 min (0.2 wt-%) with increasing nucleating additive P22 content (Figure 6). Such a decrease in t_p documents an increase in the number of predetermined nuclei,

which consequently leads to an increase in the overall crystallisation rate. As is seen in Figure 6, the width of the exothermal crystallisation peak decreases with a decrease in t_p.

At all temperatures of isothermal crystallisation in the range from 201 to 211 °C, the 0.1 wt-% nucleated sample crystallises much faster than the non-nucleated one (Figure 7), which underlines the high nucleation efficiency of the nucleating additive P22.

Furthermore, the comparison between the curves (a) and (b) in Figure 6 reveals that the presence of glass fibres enhances crystallisation. This is in agreement with results on glass fibre reinforced polyalkylene terephthalates by Chisholm and Zimmer [13].

From the linearisation of the Avrami equation, see eq. (5), two regions of different slope are obtained (Figure 8). In accordance to ref. [12], the linear range with a strong increase in the slope can be related to the primary crystallisation, followed by a slower crystallisation at larger times denoted as secondary crystallisation. The kinetics of crystallisation is seen by the intersection of the curve in the linear part with the ordinate or by the corresponding shift along the time axis with increasing crystallisation temperature. Both, the non-nucleated and the 0.1 wt-% nucleated PA 6-GF30 show a significant enhancement of crystal growth with decreasing crystallisation temperature in the range from 201 to 209 °C (Figure 8). The slope at lower crystallisation times (t), which characterises the nucleation mechanism, changes only slightly with the crystallisation temperature.

3.2.2 Hot Stage Polarised Light Microscopy (HSM)

Applying the HSM method, the spherulitic growth is described by an increase in the transmitted polarised light with increasing crystallisation time at a given crystallisation temperature from 201 to 211 °C during isothermal conditions, as is shown in Figure 9 for the non-nucleated and the 0.1 wt-% nucleated PA 6-GF30, respectively [11].

Starting in the melt, the transmitted light intensity after passing the polariser – analyser set-up at t = 0 is zero. Spherulitic growth changes the polarisation plane and leads to an increase in the transmitted light intensity reaching a plateau, where the primary crystallisation is completed (at $t = \infty$). The resulting intensity-time curves are s-shaped (Figure 9). The crystallisation temperatures were chosen to reach the maximum transmitted light intensity within the short-time range up to 20 minutes. With increasing crystallisation temperature (T_c) the curves shifts towards longer crystallisation times and the slope in the linear part decreases. The shift of the intensity-time curves can be quantified by an increase in the half-width ($t_{1/2}$) of the relative degree of crystallinity (χ_{rel}) applying equ. (8). At T_c = 211 °C, the half-width is about 7 min for the nucleated PA 6-GF30 in comparison with about 11 min for the non-nucleated one showing a strong increase in the primary crystallisation rate due to the use of the P22 nucleating additive.

3.3 Light microscopy (LM)

Light microscopical studies show a significant decrease in the size of the spherulites (diameter of less than 5 µm) together with an improved distribution

of the spherulites for the 0.1 and 0.2 wt-% nucleated in comparison to the non-nucleated (diameter 15 to 20 µm) PA 6-GF30 samples (Figures 10 and 11). Similar results have been described on the corresponding non-reinforced PA 6 [11].

3.4 Scanning Electron Microscopy (SEM)

For the discussion of the fibre matrix adhesion three representative SEM images out of a large variety of images will be used. Chosen are the non-nucleated samples prepared via tensile experiments at room temperature (Figure 12a) and at cryo conditions (Figure 12b) in comparison to a 0.2 wt-% nucleated sample prepared via tensile experiments at room temperature (Figure 12c). The SEM images reveal that in some areas of the fracture surface the polymeric matrix adheres well to the glass fibre. In other areas, the fibre surface is smooth and does not show matrix residuals, which suggests a weak fibre matrix adhesion. With respect to fibre-matrix adhesion there are no significant differences, which arise from the temperature of fracture as well as the use of nucleating additives.

3.5 Atomic Force Microscopy (AFM)

Samples cut perpendicular to the processing direction have been investigated by means of AFM using the pulsed force mode (PFM). The cross section exhibits a highly oriented skin layer and a spherulithic core region, which is in agreement to the fibre orientation measurements in Figure 5.

Topography

The topography image in Figure 13 on 0.1 wt-% nucleated PA 6-GF30 shows a morphology in the vicinity of the glass fibre, called interphase, which is different to the spherulitic structure in the polymeric matrix according to Kroh [18]. Such an interphase is also found for the non-nucleated and the 0.2 wt-% nucleated PA 6-GF30. The thickness is in the range between 1.4 and 2.9 µm showing no definite correlation with the nucleating additive content. According to Kocker [20] it is known that the interphase layer thickness has a direct influence on the shear strength in single fibre pullout tests and therefore, the thermo-mechanical composite properties.

Adhesion

Applying the PFM mode, the adhesion image shows the highest contrast. That originates from the minimal force of the force-to-distance curve leading to a very clear signal, which contains additional information compared to that of the topography image. The adhesion image in Figure 14 on 0.2 wt-% nucleated PA 6-GF30 confirms the existence of an interphase already seen in the topography image in Figure 13. Additionally, the adhesion image suggests that the interphase consists of a transcrystalline layer besides a sizing layer [18]. With respect to Harel and Maron [21], the phenomenon of transcrystallisation can take place if the nuclei density at the fibre surfaces exceeds that in the polymer matrix.

3.6 Martens Heat Deflection Temperature

The non-nucleated PA 6-GF30 has shown an averaged heat deflection

temperature according to Martens of 145 °C, represented in Figure 15. Both nucleated samples exhibit significant higher heat deflection temperatures with 155 °C and 164 °C for the 0.1 and 0.2 wt-% nucleated samples, respectively [18]. It is assumed that the increase in the heat deflection temperature with nucleating additive content is due to the strong decrease in the spherulite size and improvement in the spherulite distribution, which may support the fibre-to-matrix contact in the vicinity of the fibres.

4 Conclusions

A new type of nucleating additive Brueggolen® P22, based on the polymeric short chain polyamide (PA 2.2), has been studied with respect to the effect of the additive content (0, 0.1 and 0.2 wt-%) on the crystallisation behaviour in short glass fibre reinforced polyamide 6 composites. The resulting fibre orientation distribution has been intensely investigated. Applying the same processing conditions, there is only a minor difference in the fibre orientation.. Isothermal crystallisation experiments (DSC) using the time-to-peak temperature (t_p) have shown a significant increase in the overall crystallisation rate with both the glass fibre filler and the nucleating agent content. With respect to the linearised Avrami equation large changes in the kinetics of crystallisation are discussed. Isothermal hot stage microscopical studies show a significant enhancement of the spherulitic growth rate with decreasing crystallisation temperature and the use of the P22 nucleating additive. Light microscopically studies reveal a decrease in the spherulite size and an improvement in the spherulite distribution with heterogeneous nucleation. From AFM investigations the existence of an interphase consisting of a

transcrystalline layer in the vicinity of the glass fibre is discussed. The Martens heat deflection temperature is found to increase significantly with nucleating additive content, probably supported by an improved fibre-to-matrix contact in relation to the spherulite size and distribution.

Acknowledgement

The authors would like to thank K. Titzschkau and P. Beck (BrüggemannChemical) for the materials and processing. Financial support is acknowledged from the “Max Buchner Stiftung” in the frame of the project 2459 ("Verbesserte Wärmeformbeständigkeit thermoplastischer Mehrphasenwerkstoffe durch kontrolliertes Kristallwachstum"). Furthermore, the authors thank the co-workers at the Institute for Polymer Technology (IKT), Germany S. Osterloh, U. Müller and U. Fritz and the former students M. Kroh and S. Moritz for their substantial technical support.

References

[1] Alfonso GC, Ziabicki A. Memory effects in isothermal crystallization, II. Isotactical polypropylene, Coll Polym Sci 1995; 273: 317-323

[2] Tizschkau K, Beck P. Processing auxiliaries for polyamides, nucleation – lubrication – chain length modification, POLAMIDE 2001: 2nd World Congress Conference Proceedings, Düsseldorf, Germany, 2001, p 1-20.

[3] Mudra I, Balazs G. Comparative study of efficiency of nucleating agents in PA-6, J Therm Analysis Calorimetry 1998; 52 (2): 355-361

[4] Brink T, Cohen JL, Sham CK. Process for the production of polyamide moulded parts with improved crystallisation behaviour, PCT Int. Appl. WO 9824846, CAN 129:068613

[5] Gurato G, Gaidano DG, Zannetti R, Influence of nucleating agents on the crystallization of 6-polyamide, Makromol Chem 1978; 179 (1): 231-245

[6] Fracassi A, Göschel U, Titzschkau K. Crystal growth in nucleated polyamide PA 6, 18. Stuttgarter Kunststoffkolloquium Conference Proceedings, 2003, 5P2

[7] Göschel U, Fritz U, Davidson NC, Lutz W, Buth G. Crystallisation kinetics in nucleated polyamides, project PX 03-003, ANKA Synchrotron Radiation Facility, Annual Report Karlsruhe, Germany, 2004

[8] Fracassi A. Improvement of warpage of glass fibre-reinforced polyamide (PA 6-GF) composites by means of well-defined nucleation, Diploma Thesis, University of Stuttgart, Germany, Institute for Polymer Testing and Polymer Science (IKP), 2003

[9] Davidson NC. Image analysis for fibre orientation measurement, Ph.D. thesis, University of Leeds, U.K., 1993

[10] Davidson NC, Clarke AR, Archenhold GA. Large area high resolution Image analysis of composite materials, J Microscopy 1997; 185 (2): 233-242

[11] Moritz S. Crystallisation kinetics on glass fibre reinforced polyamide materials (German), Student Thesis, University of Stuttgart, Germany, Institute for Polymer Testing and Polymer Science (IKP), 2004

[12] Azzurri F. Melt crystallization and polymorphic transformation in isotactic poly (1-butene) based materials, PhD. thesis, University of Genoa, Italy, 2003

[13] Chisholm BJ, Zimmer JG. Isothermal crystallization kinetics of commercially important polyalkylene terephthalates, J Appl Polym Sci 2000; 76 (8): 1296-1307

[14] Hiemenz PC. Polymer Chemistry, Marcel Dekker, New York, 1984

[15] Verhoven O. Crystallization of polyethylene terephthalathe in injection moulding, PhD thesis, Université Catholique de Louvain, Belgium, 1997

[16] Krotil HU, Stifter T, Waschipky H, Weishaupt K, Hild S, Marti O. Pulsed force mode: a new method for the investigation of surface properties, Surface and Interface Analysis 1999; 27 (5-6): 336-340

[17] Grandy DB, Hourston DJ, Price DM, Reading M, Silva GG, Song M, Sykes P. Microthermal characterization of segmented polyurethane elastomers and a polystyrene-poly (methyl methacrylate) polymer blend using variable-temperature pulsed force mode atomic force microscopy, Macromolecules 2000; 33: 9348-9359

[18] Kroh M. Investigation of the structure of glass fibre reinforced polyamide using atomic force microscopy (AFM) (German), Student Thesis,

University of Stuttgart, Germany, Institute for Polymer Testing and Polymer Science (IKP), 2004

[19] Wunderlich B. Macromolecular Physics: Crystal structure, morphology, defects, 1, Academic Press, New York, 1973, p. 389.

[20] Kocker K. A new test method for the determination of the fibre/matrix adhesion of fibre reinforced thermoplastic resins, PhD thesis, RWTH Aachen, Germany, 1996

[21] Harel H, Maron G. On crystalline interfaces in composite materials, Acta Polym 1998; 49: 583 – 587

Figure captions

Figure 1: Monomeric unit of PA 2.2.

Figure 2: Samples taken from a tensile bar (DIN EN ISO 527) for fibre orientation, SEM and AFM studies.

Figure 3: Temperature profile for the isothermal crystallisation studies at different crystallisation temperatures (T_c).

Figure 4: Coordinate system for the rectangular plate.

Figure 5: Fibre orientation distribution in the plane 2-3 of a 0.1 wt-% nucleated PA 6-GF30 rectangular plate. The 1-direction is in processing direction, in analogy to Figure 4.

Figure 6: DSC traces of isothermal crystallisation of (a) non-nucleated and non-reinforced PA 6, (b) non-nucleated PA 6-GF30, (c) 0.1 wt-% nucleated PA-GF30 and (d) 0.2 wt-% nucleated PA 6-GF30, studied at a crystallisation temperature of 205 °C subsequent to a fast cooling from the molten state at 265 °C.

Figure 7: Time-to-peak temperature (t_p) from DSC exothermal crystallisation peak of (a) non-nucleated and (b) 0.1 wt-% nucleated PA 6-GF 30 at different temperatures of isothermal crystallisation ranging from 201 to 211 °C [11].

Figure 8: Linearised Avrami plot from DSC measurements of the non-nucleated and the 0.1 wt-% nucleated PA 6-GF30 at temperatures of isothermal crystallisation ranging from 201 to 209 °C [11].

Figure 9: Transmitted light intensity vs. crystallisation time from HSM measurements of 0.1 wt-% nucleated PA 6-GF30 at temperatures of isothermal crystallisation ranging from 201 to 211 °C. In comparison the non-nucleated PA 6-GF30 at 211 °C is represented [11].

Figure 10: LM image, non-nucleated PA 6-GF30 at T_c = 209 °C.

Figure 11: LM image, 0.1 wt-% nucleated PA 6-GF30 at T_c = 209 °C.

Figure 12a: SEM image of non-nucleated PA 6-GF30 prepared via fracture at room temperature.

Figure 12b: SEM image of non-nucleated PA 6-GF30 prepared via fracture at cryo conditions.

Figure 12c: SEM image of 0.2 wt-% nucleated PA 6-GF30 prepared via tensile experiment at room temperature.

Figure 13: Left: AFM (PFM) image of 0.1 wt-% nucleated PA 6-GF30, topography. Right: Scheme of the interphase layer [18].

Figure 14: a) AFM (PFM) image of 0.2 wt-% nucleated PA 6-GF30, adhesion, b) Scheme of the interphase layer in accordance to ref. [18].

Figure 15: Heat deflection temperature of non-nucleated as well as 0.1 and 0.2 wt-% nucleated PA 6-GF30 [18].

Tables

Table 1: Parameters chosen in the injection moulding processing.

Parameters	Tensile bars (DIN EN ISO 527)	Rectangular plates (DIN EN ISO 294-4)
Melt temperature (°C)	265	265
Holding pressure (MPa)	50	45
Holding time (sec)	9	7
Mould temperature (°C)	70	70
Cooling time (sec)	10	9
Cycle time (sec)	25.9	22.5

Table 2: Fibre orientation in PA 6-GF30 tensile bar samples of different P22 nucleating additive content.

Additive content (wt-%)	a_{11}	a_{22}	a_{33}
0	0.677	0.201	0.123
0.1	0.692	0.193	0.116
0.2	0.700	0.188	0.111

Table 3: Melting and crystallisation parametres of PA 6-GF30 tensile bar samples of different P22 nucleating additive content from DSC measurements.

Additive content (wt-%)	Melting peak temperature T_m (°C)	Melting enthalpy ΔH (J/g)	Degree of crystallinity χ (%)	Onset of crystallisation $T_{c,\ onset}$ (°C)
0	221.9	42.2	32.0	192.4
0.1	221.9	42.9	32.5	194.1
0.2	222.4	42.7	32.4	194.6

Figures

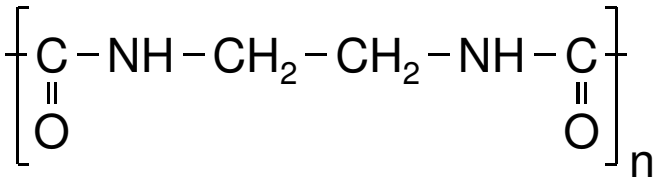

Figure 1: Monomeric unit of PA 2.2.

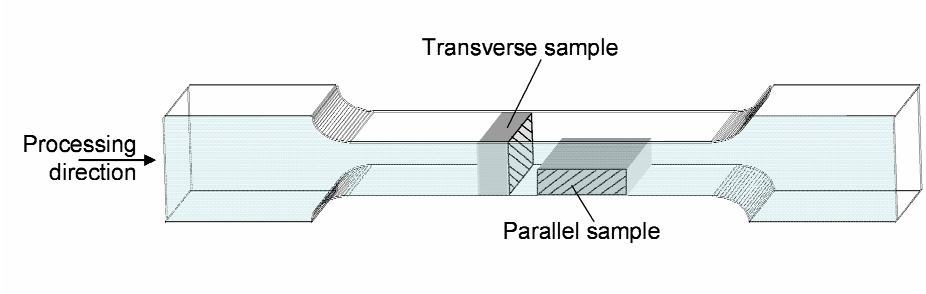

Figure 2: Samples taken from a tensile bar for fibre orientation, SEM and AFM studies.

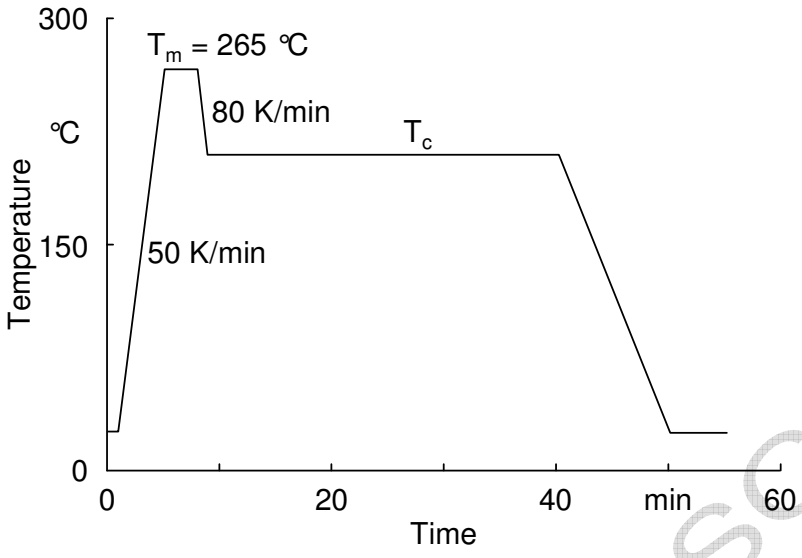

Figure 3: Temperature profile for the isothermal crystallisation studies. Here, a crystallisation temperature of T_c = 209 °C is applied.

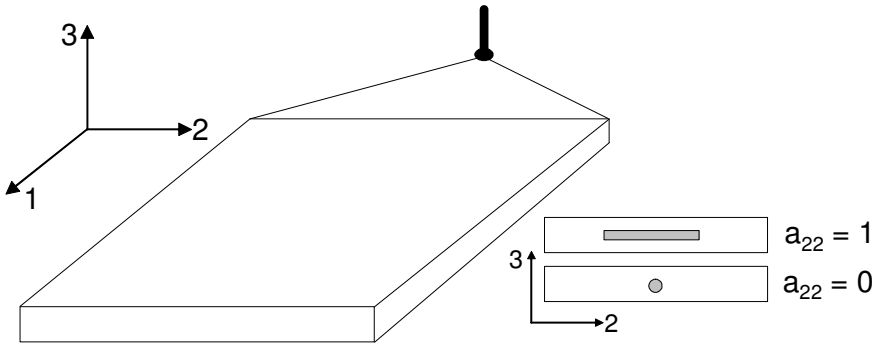

Figure 4: Coordinate system for the rectangular plate.

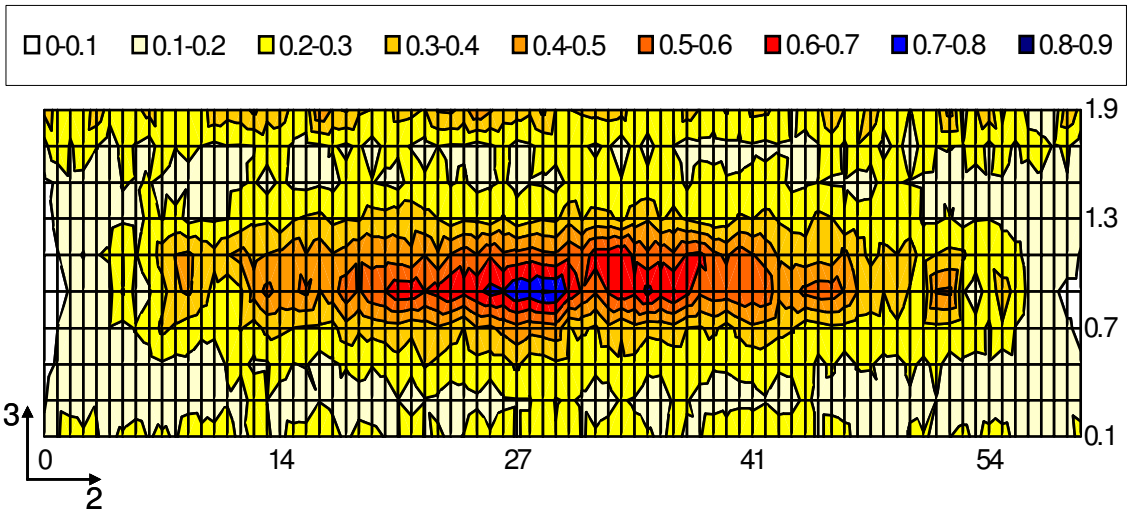

Figure 5: Fibre orientation distribution in the plane 2-3 of a 0.1 wt-% nucleated PA 6-GF30 rectangular plate. The 1-direction is in processing direction, in analogy to Figure 4.

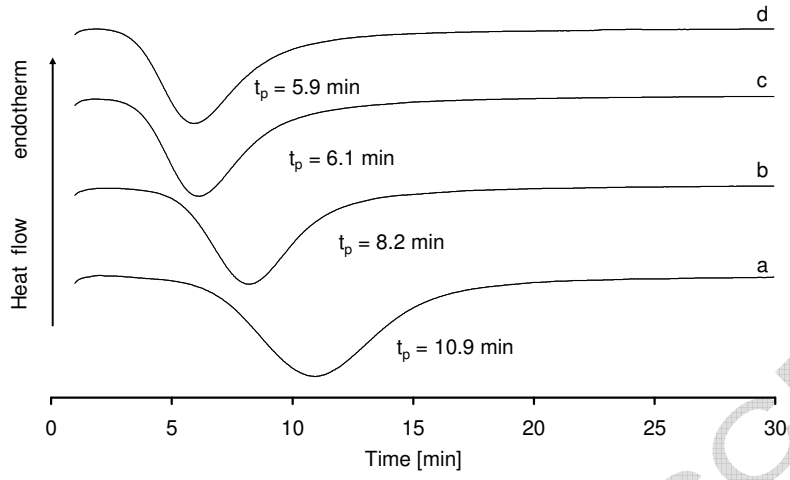

Figure 6: DSC traces of isothermal crystallisation of (a) non-nucleated and non-reinforced PA 6, (b) non-nucleated PA 6-GF30, (c) 0.1 wt-% nucleated PA-GF30 and (d) 0.2 wt-% nucleated PA 6-GF30, studied at a crystallisation temperature of 205 °C subsequent to a fast cooling from the molten state at 265 °C.

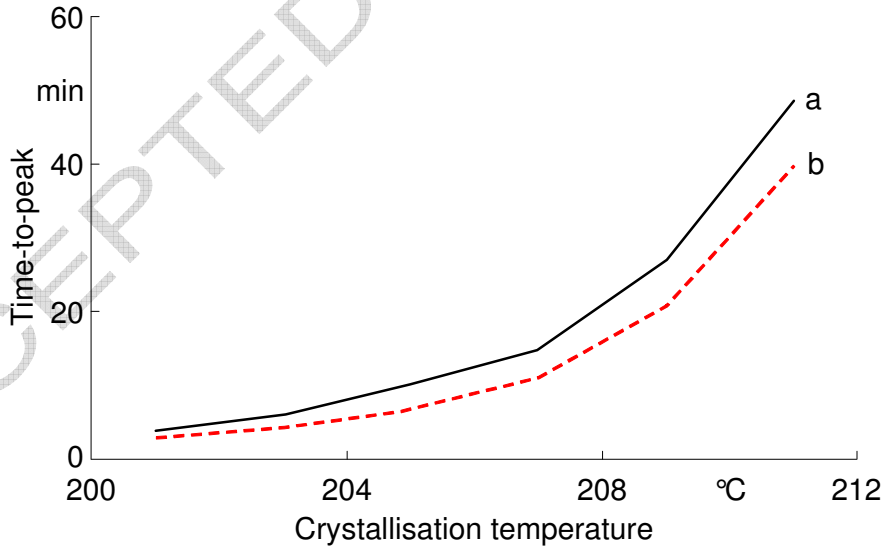

Figure 7: Time-to-peak temperature (t_p) from DSC exothermal crystallisation peak of (a) non-nucleated and (b) 0.1 wt-% nucleated PA 6-GF 30 at different temperatures of isothermal crystallisation ranging from 201 to 211 °C [11].

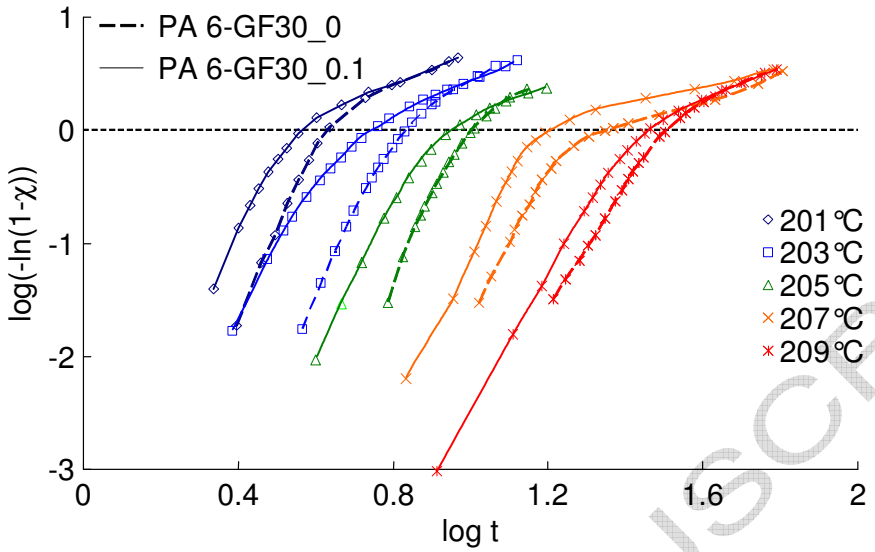

Figure 8: Lineralised Avrami plot from DSC measurements of the non-nucleated and the 0.1 wt-% nucleated PA 6-GF30 at temperatures of isothermal crystallisation ranging from 201 to 209 °C [11].

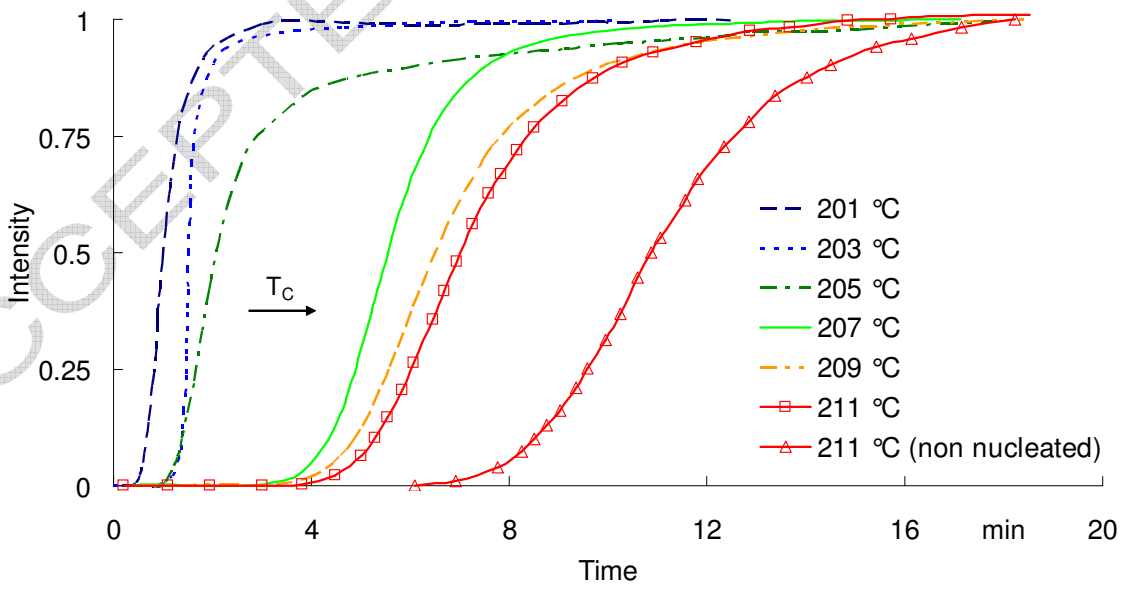

Figure 9: Transmitted light intensity vs. crystallisation time from HSM measurements the 0.1 wt-% nucleated PA 6-GF30 at temperatures of

isothermal crystallisation ranging from 201 to 211 °C. In Comparison the non-nucleated PA 6-GF30 at 211 °C is represented [11].

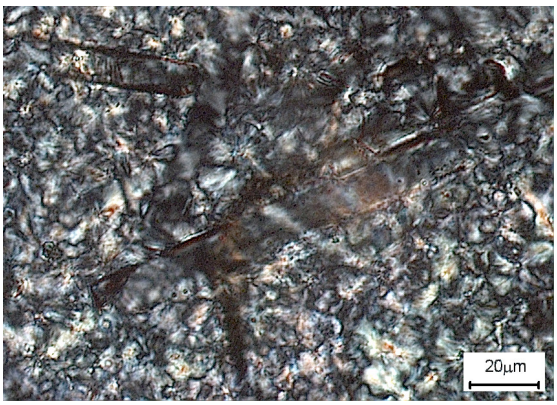

Figure 10: LM image, non-nucleated PA 6-GF30 at T_c = 209 °C.

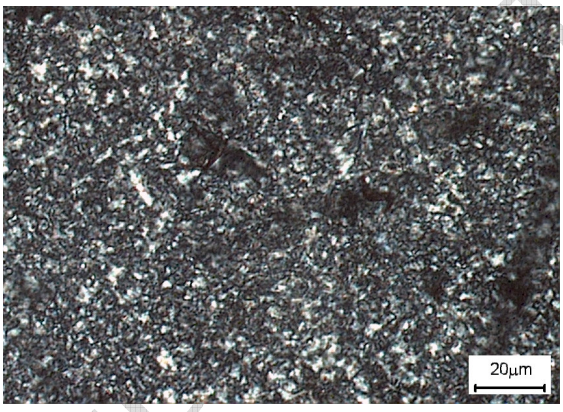

Figure 11: LM image, 0.1 wt-% nucleated PA 6-GF30 at T_c = 209 °C.

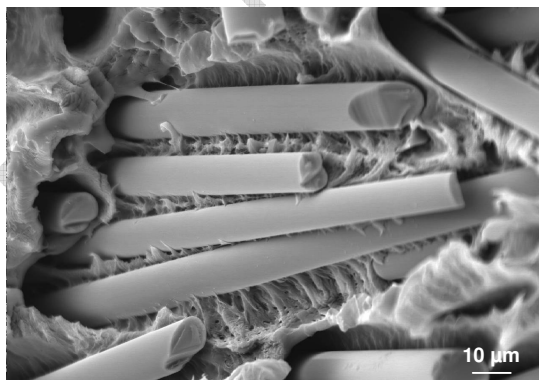

Figure 12a: SEM image of nonnucleated PA 6-GF30 prepared via fracture at room temperature.

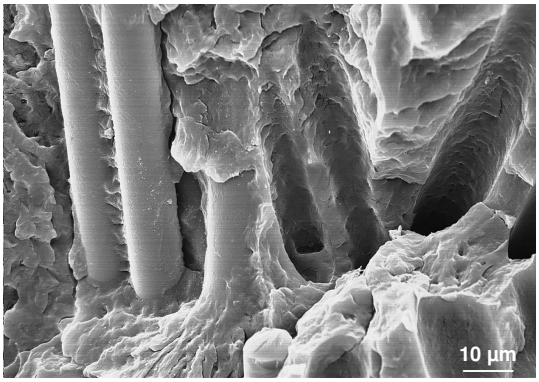

Figure 12b: SEM image of nonnucleated PA 6-GF30 prepared via fracture at cryo conditions.

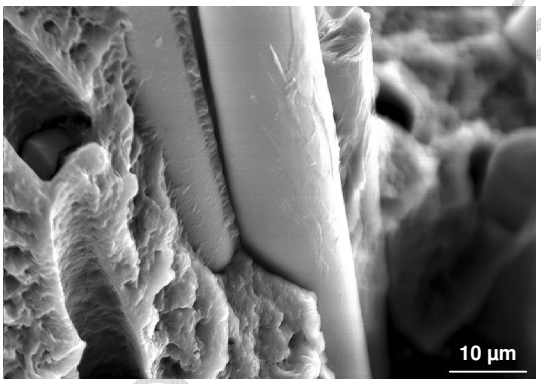

Figure 12c: SEM image of 0.2 wt-% nucleated PA 6-GF30 prepared via fracture at room temperature.

.

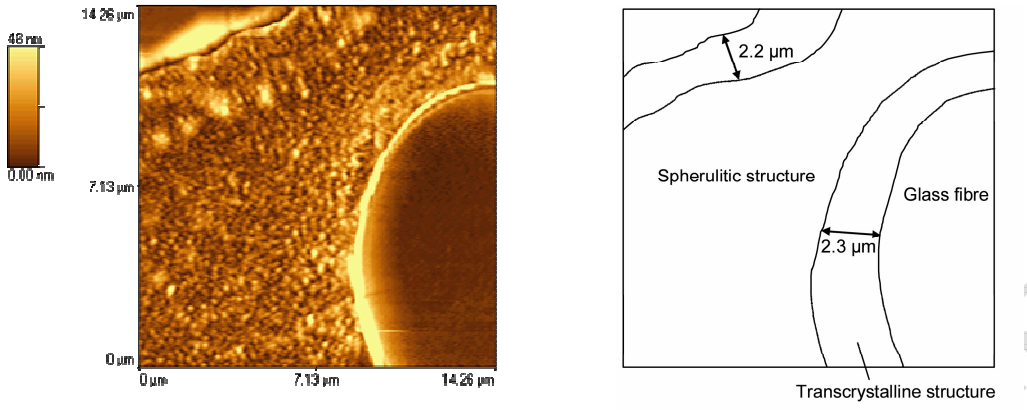

Figure 13: Left: AFM (PFM) image of 0.1 wt-% nucleated PA 6-GF30, topography. Right: Scheme of the interphase layer [18].

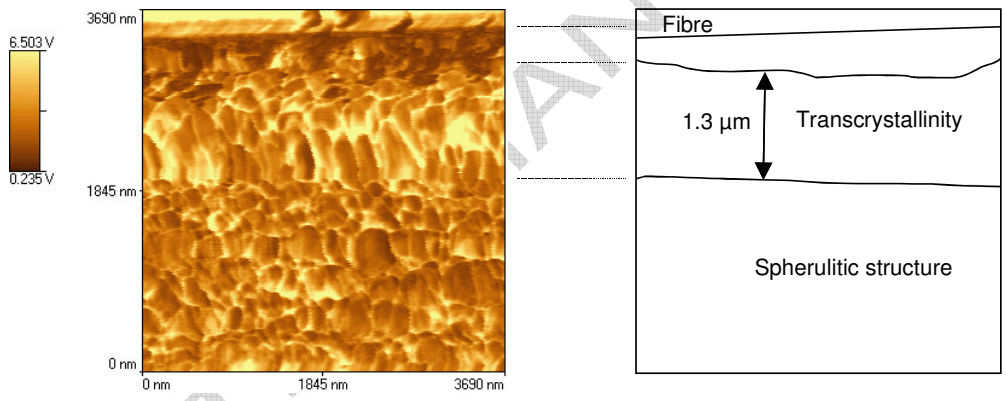

a) b)

Figure 14: a) AFM (PFM) image of 0.2 wt-% nucleated PA 6-GF30, adhesion, b) Scheme of the interphase layer in accordance to ref. [18].

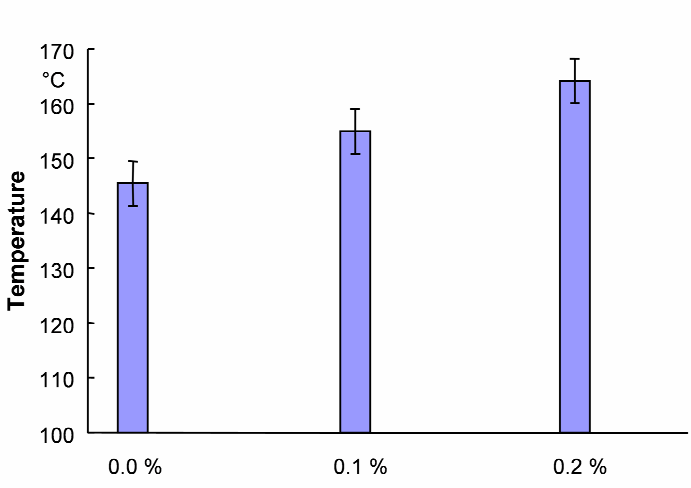

Figure 15: Heat deflection temperature of non-nucleated (0.0 wt-%) as well as 0.1 and 0.2 wt-% nucleated PA 6-GF30 [18].